

VIKIN: A Reconfigurable Accelerator for KANs and MLPs with Two-Stage Sparsity Support

Wenhui Ou, Zhuoyu Wu, Yipu Zhang, Zheng Wang and C. Patrick Yue

Abstract—The commonly used Multi-layer Perceptrons (MLPs) in modern AI applications significantly limit the real-time performance due to their intensive memory access operation. Recently, Kolmogorov–Arnold Networks (KANs) have gained attention for offering a similar structure to MLPs but with a more efficient parameter utilization. However, the lack of customized support in conventional hardware restricts the performance gain from its algorithmic superiority. Furthermore, the limited applicability of KANs in edge scenarios, especially where MLPs excel, makes dedicated hardware for KANs inefficient and impractical. In this work, we present VIKIN, a reconfigurable accelerator that enables efficient inference for both KANs and MLPs using unified hardware, providing flexibility to handle diverse edge workloads. Apart from its pipeline mode and two-stage sparsity support for efficient KAN processing, VIKIN can also improve the throughput of MLPs with the same sparsity support in parallel mode. Experiments on a real-world dataset show that VIKIN provides a $1.28\times$ acceleration and a 19.58% reduction in accuracy loss by replacing MLPs with KANs. For a more accurate KAN model version with $3.29\times$ operation, the latency overhead on VIKIN is only $1.24\times$ compared to the baseline KAN model. Additionally, VIKIN achieves a $1.25\times$ speed-up and $4.87\times$ energy efficiency compared to a common edge GPU when performing KAN model.

Index Terms—Kolmogorov-Arnold Networks, Reconfigurable Accelerator, Sparsity

I. INTRODUCTION

Multi-layer Perceptrons (MLPs) are widely adopted and serve as fundamental building blocks in advanced neural networks, due to their simple structure and strong versatility. However, the same factors that make MLPs attractive also lead to inherent limitations. First, the poor weight reuse and the large number of parameters required for satisfactory accuracy impose significant pressure on memory bandwidth, making MLPs a bottleneck on hardware. For example, in a specialized Transformer accelerator [4], MLPs account for up to 60% of the total latency and energy consumption. Second, MLPs are essentially black-box models with limited interpretability [27], making it difficult to obtain feedback for network optimization after training. These limitations motivate the exploration of emerging alternatives.

Recently, Kolmogorov–Arnold Networks (KANs) [8] have emerged as a competitive alternative to MLPs. Specifically,

This work was supported by Hong Kong Research Grants Council through the Areas of Excellence (AoE) Scheme under Grant AoE/E-601/22-R and NSFC under Grant No. 62372442. (Corresponding author: C. Patrick Yue.)

Wenhui Ou, Yipu Zhang, and C. Patrick Yue are with the Department of Electronic and Computer Engineering, The Hong Kong University of Science and Technology, Hong Kong SAR, China.

Zhuoyu Wu is with the School of IT, Monash University, Malaysia Campus, and Zheng Wang is with the Shenzhen Institutes of Advanced Technology, Chinese Academy of Sciences, Shenzhen, China.

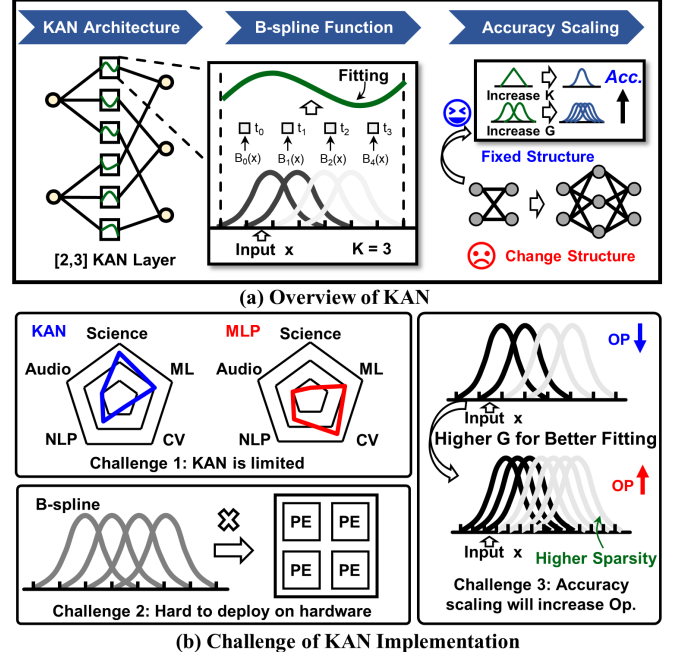


Fig. 1. (a) Overview of KAN and (b) its implementation challenges. In (a), we show an example of a [2,3] KAN layer, where the output is constructed by linearly combining multiple B-spline basis functions with learnable weights. The use of B-splines enables accuracy scaling by tuning spline parameters instead of changing the model structure. In (b), the comparison between KAN and MLP is summarized based on [6], highlighting the need for unified hardware that can efficiently support both models.

KANs retain the same high-level architecture as MLPs, making them a drop-in replacement in different neural networks (NNs). Moreover, in certain cases, KANs can deliver higher accuracy while using fewer parameters compared to MLPs [8]. Most importantly, by introducing B-spline functions [11] as key components, KANs not only improve interpretability but also enable a smoother accuracy-scaling mechanism, where accuracy can be enhanced by tuning internal parameters instead of redesigning the overall NN architecture, as shown in Fig. 1(a). Recent studies have verified that the integration of KANs can improve the performance of mainstream models such as Transformers [9] and LSTMs [10], further demonstrating their potential for broader deployment.

Nevertheless, Bringing the algorithmic benefits of KANs to hardware, especially edge devices in diverse workload environments, still faces several challenges, as shown in Fig. 1(b): (1) According to the latest survey [6], the benefits of KANs are confined to specific applications, such as scientific tasks, while their performance in other domains remains limited, indicating that KANs cannot yet fully replace MLPs across all workloads; (2) Existing high-parallelism hardware accelerators

are typically based on processing element (PE) arrays [7], which are well-optimized for MLPs but struggle to support KANs due to the unique computations involved in B-spline functions; (3) Although KANs allow smoother accuracy scaling without changing the architecture, they also introduce significant operation overhead, which can sometimes exceed those of MLPs and may counteract the efficiency gains.

To address the aforementioned challenges, we make the following contributions in this paper:

- We propose **VIKIN**, a versatile inference engine that can operate in two modes: a pipeline mode for KANs, and a parallel mode for MLPs, to adapt to varying workload characteristics with unified hardware.
- We design a reconfigurable B-spline Unit (SPU) that can efficiently execute B-spline functions with different parameter settings, while it can also be reused for MLPs to enhance hardware utilization.
- We integrate dedicated sparsity support to optimize KAN’s accuracy-scaling capability, which can significantly reduce computational overhead of more accurate KAN models, while MLPs can also benefit from this.
- Experimental results show that, compared with a common edge GPU, KAN achieves a $1.25\times$ speedup and a $4.87\times$ improvement in energy efficiency on our dedicated engine, whereas MLPs also benefit from our design, achieving a $2.20\times$ energy saving.

II. PRELIMINARY

A. Kolmogorov Arnold Networks

KAN was derived from the Kolmogorov-Arnold representation theorem [13], which was originally composed of two layers. A KAN layer $\phi_{q,p}$ with n_{in} inputs and n_{out} outputs [8] can be defined as:

$$\Phi = \{\phi_{q,p}\}, p = 1, 2, \dots, n_{in}, q = 1, 2, \dots, n_{out} \quad (1)$$

The KAN layers can be generalised in Eq. 2, where $\text{silu}(x) = x/(1 + e^{-x})$ and $\text{spline}(x) = \sum_{i=0}^m c_i B_i(x)$, with learnable weights w_b and w_s . Using the similar fully-connected structure of MLPs, KANs can be expanded to any L layers with the output expressed as $\text{KAN}(x) = \Phi_{L-1} \circ \Phi_{L-2} \cdots \circ \Phi_0 \circ x_0$ [8].

$$\phi(x) = w_b \text{silu}(x) + w_s \text{spline}(x) \quad (2)$$

For hardware-friendly implementation, the learnable weight w_s can be combined with c_i to form $t_i = w_s c_i$

$$\phi(x) = w_b \text{silu}(x) + \sum_{i=0}^m t_i B_i(x) \quad (3)$$

Fig. 1(a) illustrates a KAN layer with 2 inputs and 3 outputs (denoted as $[2, 3]$). The computation can be conceptually divided into two stages: (1) the SiLU activations and B-spline basis functions $B_i(x)$ are first computed; (2) the resulting intermediate values are processed via multiply-and-accumulate (MAC) operations using learnable weights w_b and t_i . Since each input generates $(m+1)$ intermediate result in the first stage, the second stage can be viewed as a linear layer of an

MLP with dimensions $[2 \cdot (m+1), 3]$. Here, m represents the number of B-spline basis, as shown in Eq. 3.

B. B-Spline Functions and Accuracy Scaling

KAN employs B-spline functions to approximate nonlinear mappings by combining localized basis components $B_i(x)$ with trainable coefficients t_i (Fig. 1(a)) [11]. A B-spline basis is specified by the spline order K and the knot/grid positions $\{x_i\}$ (grid size G determines the number of knot placements within a fixed input interval). The zero-order basis is

$$B_{0,i}(x) = \begin{cases} 1 & x_i \leq x < x_{i+1}, \\ 0 & \text{otherwise} \end{cases} \quad (4)$$

and higher-order bases can be recursively computed from lower-order ones:

$$B_{K,i}(x) = \frac{x - x_i}{x_{i+K} - x_i} B_{K-1,i}(x) + \frac{x_{i+K+1} - x}{x_{i+K+1} - x_{i+1}} B_{K-1,i+1}(x) \quad (5)$$

This parametrization allows accuracy to be scaled in two ways, as shown in Fig. 1(a): using a larger K for smoother and more expressive bases, or increasing G to obtain more fine-grained local fitting, all without changing the model architecture. In particular, enlarging only G offers a lightweight way to boost accuracy without retraining the model from scratch [8]. Although a larger G increases the number of $B_i(x)$ evaluations, it also leads to higher sparsity, since $B_i(x)$ becomes zero when x lies outside its local support, as illustrated in Fig. 1(b). This sparsity can be effectively exploited to reduce computational overhead.

III. OVERALL ARCHITECTURE

Fig. 2 shows the overall architecture of VIKIN. Like most accelerators [14], it operates alongside a host processor that handles configuration and issues flexible control instructions. A global buffer stores most weight data and provides high bandwidth, avoiding frequent off-chip DDR access and ensuring sufficient data supply for inference.

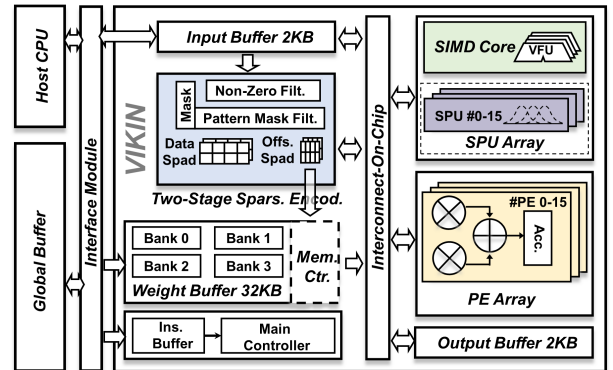


Fig. 2. Overall hardware architecture of VIKIN.

The core of VIKIN includes a SIMD core [1] for $\text{silu}(x)$, a 16-unit B-spline unit (SPU) array for computing $B_i(x)$, and a

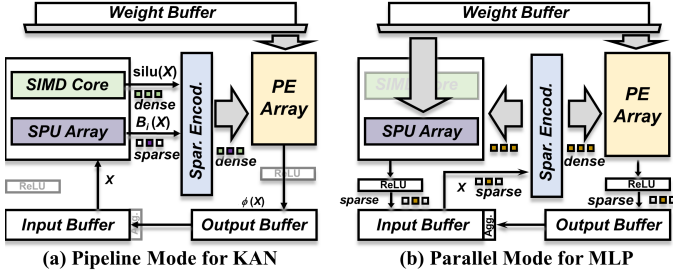


Fig. 3. The illustration of the reconfigurable dataflow: (a) pipeline mode for KAN, (b) parallel mode for MLP.

16-unit processing element (PE) array for MAC operations, as outlined in Eq. 3. Additionally, a two-stage sparsity encoder (TSE) supports sparsity-aware computation in both parallel and pipeline modes. To optimize performance for accuracy-sensitive applications [16], [17], KAN inference is performed in FP16, striking a balance between speed and accuracy.

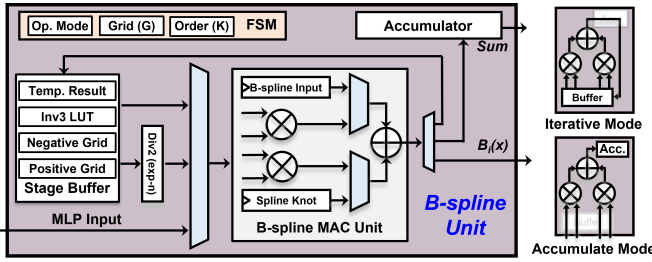


Fig. 4. The hardware architecture of the reconfigurable B-spline unit (SPU) supports two modes: iterative mode for B-spline bases $B_i(x)$ in KAN, and accumulation mode, which functions as a PE for MLP.

IV. RECONFIGURABLE MODE AND MICROARCHITECTURE

A. Reconfigurable Dataflow

VIKIN supports two operation modes. In pipeline mode for KANs, as shown in Fig. 3(a), the SIMD core and SPU array process input data from the input buffer. Since $B_i(x)$ is bounded, the SPU array produces sparse outputs with many zeros. The TSE forwards only the non-zero $B_i(x)$ results to the PE array, which then writes outputs directly to the output buffer, bypassing the ReLU block.

In parallel mode for MLPs (Fig. 3(b)), the interconnect reconfigures the hardware to connect the input buffer directly to the TSE. The SPU array will function like PE array to perform MAC operations. SPU outputs are stored back in the input buffer, while PE outputs go to the output buffer before aggregation into the input buffer for the next layer. Reusing the TSE converts sparse MLP inputs from preceding ReLU activations into a dense format, enabling efficient sparsity-aware computation with minimal reconfiguration overhead.

B. Reconfigurable B-spline Unit

The hardware implementation of B-spline functions faces two main challenges. First, computing B-spline bases incurs high operation overhead (Eq. 5). Although LUTs can speed up computation, their performance is limited by the need to refill them whenever layer configurations change (G and K), resulting in high memory access costs, especially in dynamic

workloads. Second, the unique computation paradigm of B-splines results in highly customized hardware, which can lead to low utilization if it cannot be reused for other operations.

To improve efficiency, the SPU design incorporates several optimizations, as shown in Fig. 4: (1) We follow the computation paradigm of EfficientKAN [2] with higher speed. (2) Differences between the input and knots (i.e., $x - x_i$ and $x_{i+K+1} - x$ in Eq. 5) are computed once for the zero-order ($K=0$) basis and stored in a stage buffer, then reused for higher-order bases, thereby reducing workload by 21%. (3) Additionally, G is restricted to 2, 4, 8, 16 and K to 1, 2, 3, 4, allowing costly FP divisions in Eq. 5 to be replaced with integer operations and an LUT for the value $1/3$.

To enable reuse for MLPs and improve hardware utilization, SPUs support two modes. In iterative mode, SPUs compute higher-order $B_i(x)$ by fetching lower-order ones from the stage buffer. In accumulation mode for MLP operations, SPUs receive external inputs and use accumulators to perform MAC. Compared to the 16 nodes per batch in KAN pipeline mode, using the SPU array doubles the number of output nodes per batch for MLPs, allowing up to 32 nodes.

C. Pipeline Mode with Sparsity Support

The pipeline mode for KAN operates in two stages to hide SPU latency, while performing sparsity-aware computation. In the first stage, each SPU fetches one input, while the SIMD core processes 16 inputs in parallel. To exploit the irregular sparsity introduced by the SPU, a zero-free data format [19] is employed. As shown in Fig. 5 (a), the TSE is divided into 16 slices, each storing non-zero outputs from an SPU in the dense data Scratchpad (Spad).

In the second stage, the Spads are grouped into two sets, providing dense input to multipliers in the PEs, and offsets are sent to the weight buffer to fetch corresponding weights. Therefore, the sparsity is utilized for skipping unnecessary computation. Notably, the weight buffer dynamically adjusts its access scheme based on the operating mode. For KAN, two banks in the buffer are stacked as a group to deliver more weight data per batch for PE array, whereas in MLP mode, all four banks operate simultaneously to meet the bandwidth requirements for both the PE and SPU arrays (Fig. 5(b)).

In addition to zero-free sparsity, user-configurable sparsity is supported. The TSE filters elements in batches of four, retaining only those specified by a mask defined during model training [23], [24]. For example, with a pattern mask of 1 0 1 0, only nodes at indices 2'b00 and 2'b10 are retained if their values are non-zero (Fig. 5(a)). This two-stage sparsity strategy can reduce the PE array's computation by up to 87.5%, enabling efficient accuracy scaling for KAN.

V. EXPERIMENTAL RESULTS

In this section, we evaluate the VIKIN workflow in three steps: first, we create benchmark models based on a real-world dataset; second, we analyze performance gains from hardware optimizations, including the reconfigurable SPU and two-stage sparsity support; finally, we deploy the VIKIN prototype on an FPGA for overall evaluation.

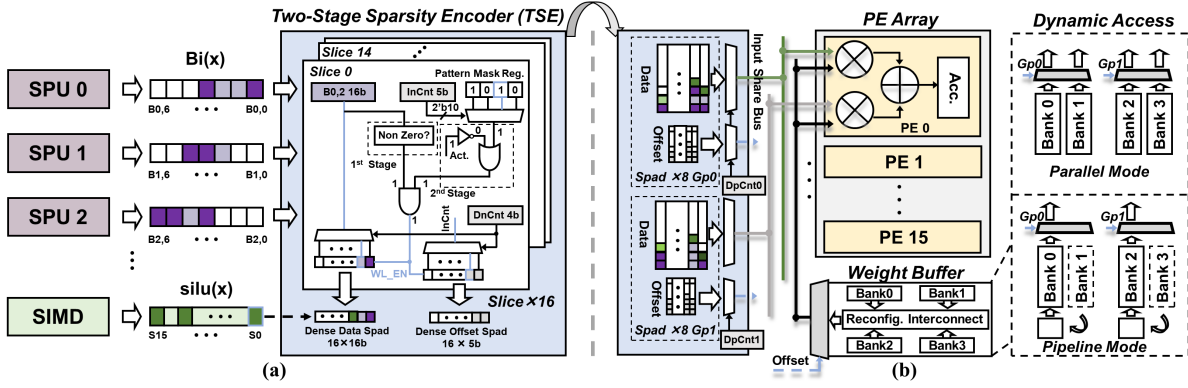


Fig. 5. The pipeline mode with sparsity support: (a) pipeline stage 1, (b) pipeline stage 2. This mode hides SPU latency through pipeline processing and reduces PE array operations via sparsity-aware computation in the TSE. The figure also illustrates the dynamic weight buffer access scheme across different operation modes to ensure sufficient bandwidth.

TABLE I
COMPARISON OF MODELS ON A REAL-WORLD DATASET

Model	Layer Size	Para. Num.	Act. Config.	MSE (E-4)	RSE (E-1)	MAE (E-2)
MLP (4-layer)	[72,304,304,96]	144k	ReLU (fixed)	8.20	5.97	1.37
MLP (3-layer)	[72,304,96]	51k	ReLU (fixed)	7.92	5.86	1.29
KAN (3-layer)	[72,32,96]	43k	silu & B-spline: $G = 4$ $K = 3$	6.06	5.13	1.14
KAN (2-layer)	[72,96]	55k	silu & B-spline: $G = 4$ $K = 3$	6.20	5.19	1.19

A. Benchmark Model Setup

To create benchmark models of KANs and MLPs for hardware evaluation, we conduct experiments on the Traffic dataset [21], which contains road occupancy data collected in California during 2015–2016. This dataset is widely recognized as a benchmark for advanced time series forecasting models due to its complex temporal patterns and real-world relevance [25], [26]. Following prior work [20], we use traffic data from three consecutive days (72 hours) as input to predict traffic occupancy for the subsequent four days (96 hours). The dataset is split in a 7:2:1 ratio for training, validation, and testing, with all models trained for 100 epochs using the Adam optimizer and a learning rate of 0.001 to ensure a fair comparison.

Table I summarizes the results of the trained models across various metrics, including Mean Squared Error (MSE), Root Relative Squared Error (RSE) [21], and Mean Absolute Error (MAE). On this dataset, KAN demonstrates superior performance with the lowest error and only 29% of the parameter count compared to the 4-layer MLP. This highlights the importance of a unified hardware framework capable of integrating both models for dynamic workloads on the edge.

B. Technique Evaluation

We deployed the trained models in Table I on VIKIN to evaluate hardware performance. As shown in Fig. 6, VIKIN accelerates the two MLP models by an average of 1.30 \times by simply skipping zero activations. When the SPU operates in accumulate mode to mimic the PE, the speedup increases to a maximum of 2.17 \times compared to the baseline, which is a simplified version of VIKIN without sparsity support and only the PE array is utilized.

Fig. 7 shows the performance gains from two-stage sparsity support over zero-free only, as discussed in Sec. IV-C. With a pattern sparsity mask size of 4, the sparsity level can

range from 0% to 75%. Even with the sparsity mask disabled (0%), all models benefit from inherent sparsity. Enabling pattern sparsity further boosts performance, with the 2-layer KAN achieving up to a 2.50 \times speedup. KANs experience diminishing returns for higher sparsity rate due to a throughput mismatch between the PE and SPU arrays. Reducing values of G and K can improve this performance scaling.

KANs allow for more grids (higher G) to improve accuracy, but at the cost of significant operation overhead. We further evaluated a 3-layer KAN with different G values to analyze the impacts on hardware and algorithm performance (Fig. 8). Higher G improves detail fitting (lower MSE) but also incurs multiple times of operations. However, by leveraging the increased sparsity, VIKIN efficiently handles the more accurate model ($G = 16$, 3.29 \times the operations of $G = 2$) with only a 1.24 \times increase in latency.

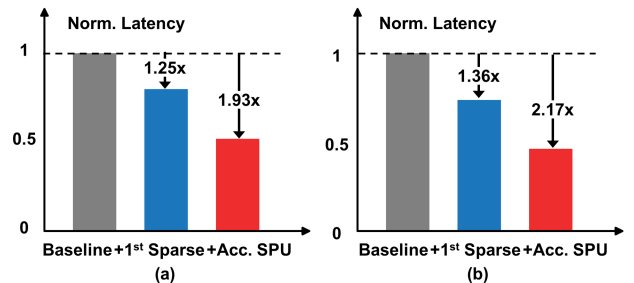


Fig. 6. The performance contribution analysis of key techniques. (a) 3-layer MLP, (b) 4-layer MLP.

C. Overall Evaluation

Table II shows the overall performance of VIKIN for executing two models, along with the hardware utilization of the Xilinx Virtex-7 VC709 operating at 115 MHz. Since the KAN model

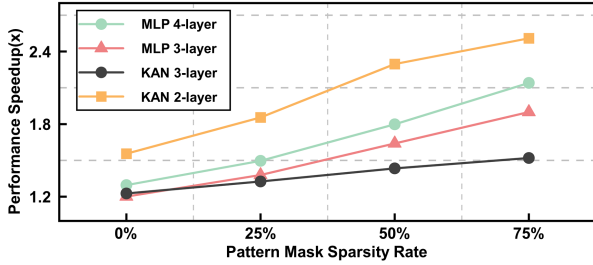


Fig. 7. The speedup performance by two-stage sparsity

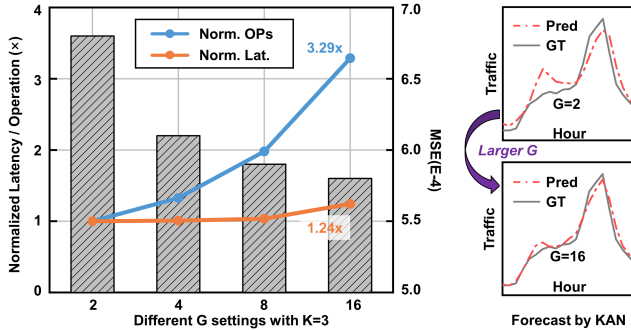


Fig. 8. The performance analysis of KAN-specific parameters

outperforms MLP in this application, VIKIN enables a 22% reduction in latency by switching from MLP to KAN on the same hardware, leveraging KAN’s superior parameter utilization and efficient computation. Furthermore, the KAN model achieves significant gains with dedicated support on VIKIN, including a 1.25 \times speedup in throughput and a 4.87 \times improvement in energy efficiency compared to a common edge GPU with more advanced process technology.

TABLE II
OVERALL EVALUATION OF SINGLE-INSTANCE VIKIN.

Model	KAN (2-layer)	MLP (3-layer)
Dataset	Traffic [21] (evaluate on FP16)	
Patt. Spar. Rate	50%	25%
Error Metrics& Rel. Error *1	MSE: 6.49 E-4 (+5%) RSE: 5.30 E-1 (+2%)	MSE: 8.07 E-4 (+2%) RSE: 5.91 E-1 (+1%)
Latency (ms)	7.47 E-3	9.56 E-3
Speed-up *2*3	1.25 \times	0.72 \times
Ener. Effi. *2*4	16.01 GOPS/W (4.87 \times)	11.34 GOPS/W (2.20 \times)
HW. Res. Util.	LUTs: 68529 FFs: 83068	DSPs: 340 BRAMs: 82

*1: The relative error is based on Table I.

*2: The Jetson Xavier NX [22], a common edge GPU with 21 TOPs peak performance, is used as the benchmark for both models in this task.

*3: Speedup represents the performance improvement in average throughput.

*4: Based on dynamic power measurements from the VC709 FPGA board.

VI. CONCLUSION

This work presents VIKIN, a reconfigurable accelerator with two-stage sparsity support, for both KANs and MLPs efficient inference. VIKIN fully exploits the strengths of KANs to enhance real-time performance which is demonstrated on a practical real-world dataset. With reconfigurable pipeline and parallel modes, VIKIN can achieve significant performance gains by simply switching dataflow on the same hardware for case-by-case operations.

REFERENCES

- [1] W. Ou, Z. Wu, Z. Wang, C. Chen, and Y. Yang, “Compact: Co-processor for multi-mode precision-adjustable non-linear activation functions,” in *2023 Design, Automation & Test in Europe Conference & Exhibition (DATE)*. IEEE, 2023, pp. 1–6.
- [2] Blealtan, “Efficientkan: An efficient implementation of kolmogorov-arnold networks,” <https://github.com/Blealtan/efficient-kan>, 2024.
- [3] S. Yu, H. Jiang, S. Huang, X. Peng, and A. Lu, “Compute-in-memory chips for deep learning: Recent trends and prospects,” *IEEE circuits and systems magazine*, vol. 21, no. 3, pp. 31–56, 2021.
- [4] F. Tu, Z. Wu, Y. Wang, L. Liang, L. Liu, Y. Ding, L. Liu, S. Wei, Y. Xie, and S. Yin, “Trancim: Full-digital bitline-transpose cim-based sparse transformer accelerator with pipeline/parallel reconfigurable modes,” *IEEE Journal of Solid-State Circuits*, vol. 58, no. 6, pp. 1798–1809, 2022.
- [5] S. S. N. Larimi, B. Salami, O. S. Unsal, A. C. Kestelman, H. Sarbazi-Azad, and O. Mutlu, “Understanding power consumption and reliability of high-bandwidth memory with voltage undervolting,” in *2021 Design, Automation & Test in Europe Conference & Exhibition (DATE)*. IEEE, 2021, pp. 517–522.
- [6] R. Yu, W. Yu, and X. Wang, “Kan or mlp: A fairer comparison,” *arXiv preprint arXiv:2407.16674*, 2024.
- [7] P. Dong, Y. Tan, X. Liu, P. Luo, Y. Liu, L. Liang, Y. Zhou, D. Pang, M.-T. Yung, D. Zhang *et al.*, “A 28nm 0.22 μ j/token memory-compute-intensity-aware cnn-transformer accelerator with hybrid-attention-based layer-fusion and cascaded pruning for semantic-segmentation,” in *2025 IEEE International Solid-State Circuits Conference (ISSCC)*, vol. 68. IEEE, 2025, pp. 01–03.
- [8] Z. Liu, Y. Wang, S. Vaidya, F. Ruehle, J. Halverson, M. Soljačić, T. Y. Hou, and M. Tegmark, “Kan: Kolmogorov-arnold networks,” *arXiv preprint arXiv:2404.19756*, 2024.
- [9] X. Yang and X. Wang, “Kolmogorov-arnold transformer,” *arXiv preprint arXiv:2409.10594*, 2024.
- [10] D. Karnehm, A. Samanta, C. Rosenmüller, A. Neve, and S. Williamson, “Core temperature estimation of lithium-ion batteries using long short-term memory (Lstm) network and kolmogorov-arnold network (kan),” *Authorea Preprints*, 2024.
- [11] W. J. Gordon and R. F. Riesenfeld, “B-spline curves and surfaces,” in *Computer aided geometric design*. Elsevier, 1974, pp. 95–126.
- [12] C. Zhou, Y. Fu, M. Liu, S. Qiu, G. Li, Y. He, and H. Jiao, “An energy-efficient 3d point cloud neural network accelerator with efficient filter pruning, mlp fusion, and dual-stream sampling,” in *2023 IEEE/ACM International Conference on Computer Aided Design (ICCAD)*. IEEE, 2023, pp. 1–9.
- [13] R. Hecht-Nielsen, “Kolmogorov’s mapping neural network existence theorem,” in *Proceedings of the international conference on Neural Networks*, vol. 3. IEEE press New York, NY, USA, 1987, pp. 11–14.
- [14] Z. Hong and C. P. Yue, “Efficient-grad: Efficient training deep convolutional neural networks on edge devices with gradient optimizations,” *ACM Transactions on Embedded Computing Systems (TECS)*, vol. 21, no. 2, pp. 1–24, 2022.
- [15] Z. Pan, Z. Gu, X. Jiang, G. Zhu, and D. Ma, “A modular approximation methodology for efficient fixed-point hardware implementation of the sigmoid function,” *IEEE Transactions on Industrial Electronics*, vol. 69, no. 10, pp. 10694–10703, 2022.
- [16] B. C. Koenig, S. Kim, and S. Deng, “Kan-odes: Kolmogorov-arnold network ordinary differential equations for learning dynamical systems and hidden physics,” *Computer Methods in Applied Mechanics and Engineering*, vol. 432, p. 117397, 2024.
- [17] M. Cheon, “Kolmogorov-arnold network for satellite image classification in remote sensing,” *arXiv preprint arXiv:2406.00600*, 2024.
- [18] W.-H. Huang, J. Jia, Y. Kong, F. Waqar, T.-H. Wen, M.-F. Chang, and S. Yu, “Hardware acceleration of kolmogorov-arnold network (kan) for lightweight edge inference,” *arXiv preprint arXiv:2409.11418*, 2024.
- [19] J. Albericio, P. Judd, T. Hetherington, T. Aamodt, N. E. Jerger, and A. Moshovos, “Cnvlutin: Ineffectual-neuron-free deep neural network computing,” *ACM SIGARCH Computer Architecture News*, vol. 44, no. 3, pp. 1–13, 2016.
- [20] C. J. Vaca-Rubio, L. Blanco, R. Pereira, and M. Caus, “Kolmogorov-arnold networks (kans) for time series analysis,” *arXiv preprint arXiv:2405.08790*, 2024.
- [21] G. Lai, W.-C. Chang, Y. Yang, and H. Liu, “Modeling long-and short-term temporal patterns with deep neural networks,” in *The 41st international ACM SIGIR conference on research & development in information retrieval*, 2018, pp. 95–104.

- [22] N. Corporation, “Jetson xavier nx,” 2023, accessed: 2025-10-28. [Online]. Available: <https://www.nvidia.com/en-us/autonomous-machines/embedded-systems/jetson-xavier-nx/>
- [23] G. Fang, H. Yin, S. Muralidharan, G. Heinrich, J. Pool, J. Kautz, P. Molchanov, and X. Wang, “Maskllm: Learnable semi-structured sparsity for large language models,” *Advances in Neural Information Processing Systems*, vol. 37, pp. 7736–7758, 2024.
- [24] M. Sun, Z. Liu, A. Bair, and J. Z. Kolter, “A simple and effective pruning approach for large language models,” *arXiv preprint arXiv:2306.11695*, 2023.
- [25] W. Cai, Y. Liang, X. Liu, J. Feng, and Y. Wu, “Msgnet: Learning multi-scale inter-series correlations for multivariate time series forecasting,” in *Proceedings of the AAAI conference on artificial intelligence*, vol. 38, no. 10, 2024, pp. 11 141–11 149.
- [26] H. Wu, J. Xu, J. Wang, and M. Long, “Autoformer: Decomposition transformers with auto-correlation for long-term series forecasting,” *Advances in neural information processing systems*, vol. 34, pp. 22 419–22 430, 2021.
- [27] F. Radenovic, A. Dubey, and D. Mahajan, “Neural basis models for interpretability,” *Advances in Neural Information Processing Systems*, vol. 35, pp. 8414–8426, 2022.